

# Nanoscopic measurements of surface recombination velocity and diffusion length in a semiconductor quantum well

V. Malyarchuk,<sup>a)</sup> J. W. Tomm, V. Talalaev,<sup>b)</sup> and Ch. Lienau

Max-Born-Institut für Nichtlineare Optik und Kurzzeitspektroskopie, Max-Born Strasse 2A,  
D-12489 Berlin, Germany

F. Rinner and M. Baeumler

Fraunhofer Institut für Angewandte Festkörperphysik, Tullastrasse 72, D-79108 Freiburg, Germany

(Received 18 April 2002; accepted for publication 15 May 2002)

We use a near-field microscopic technique to probe photoluminescence from the edge area of a quantum well. Near the edge, surface recombination gives rise to a gradual variation of the photoluminescence signal on a micrometer length scale. The overall shape in this transition region depends strongly on the excitation intensity. From solving two dimensional diffusion equations, we deduce the surface recombination velocity and the diffusion length. It is shown that the surface recombination velocity decreases with increasing intensity due to the saturation of nonradiative defect states. © 2002 American Institute of Physics. [DOI: 10.1063/1.1492307]

Surface recombination (SR) in semiconductors describes the annihilation of charge excitations at defect states near the edges of the crystal. Phenomenologically, SR is parametrized by a surface recombination velocity ( $v_s$ ) that is an important factor in characterizing the surface properties. Microscopically, the main determining factor for this surface recombination velocity is the recombination center density at the surface, which is related to the overall bulk quality of a sample.<sup>1</sup> In modern optoelectronic devices, SR is playing a more and more critical role as devices become smaller. In high power diode lasers, for example, it is well known that surface recombination increases the thermal load on the mirror surfaces, giving rise to thermal runaway and eventually limiting the lifetime of the device.<sup>2</sup> With increasing miniaturization also the diffusion length is becoming a critical factor,<sup>3</sup> defining the region of the device that is affected by surface recombination.

A variety of different techniques have been used to determine the surface recombination velocity and the diffusion length ( $L_D$ ),<sup>4–8</sup> but most of these measurements suffer from a lack of adequate spatial resolution. To unambiguously determine  $L_D$ , it is essential to probe nonequilibrium carrier concentrations with a resolution that is less than  $L_D$ , i.e., typically on the order of 1  $\mu\text{m}$  in direct band gap III/V semiconductors. The same holds true for  $v_s$ , because one needs to differentiate between the surface region and the bulk region as defined by the characteristic length scale of the diffusion length.

Photoluminescence (PL) based techniques are powerful and nondestructive probes of nonequilibrium carrier distributions and their relaxation dynamics.<sup>9</sup> Yet, the spatial resolution of far-field PL is often larger than  $L_D$ . Near-field scanning optical microscopy (NSOM), providing spatial resolution on the order of 100 nm, overcomes these limita-

tions and thus is a particularly powerful tool for the nondestructive analysis of surface recombination and diffusion processes in semiconductor devices.

In this letter, we have performed a *simultaneous* nanoscopic measurement of  $v_s$  and  $L_D$  on a semiconductor quantum well. Near field microscopy is used to probe PL in the vicinity of the edge of a quantum well sample.

The sample under investigation is a single InGaAs quantum well (QW) grown by molecular beam epitaxy on a Si-doped GaAs substrate. The 7 nm  $\text{In}_{0.16}\text{Ga}_{0.84}\text{As}$  QW is buried 220 nm below the sample surface. It is clad from both sides between 10 nm GaAs layers, surrounded by 200 nm  $\text{Al}_{0.2}\text{Ga}_{0.8}\text{As}$  barriers. After growth, the sample was cleaved in air in the direction perpendicular to the QW plane. The cleaved surface was exposed to a plasma cleaning and coating process in order to improve the surface quality.<sup>5,10</sup>

Spatially resolved near-field PL experiments are performed at room temperature using a near-field microscope [Fig. 1(a)]. The microscope is used in the illumination/collection geometry: the He-Ne excitation laser (photon energy 1.96 eV) is transmitted through the near-field fiber probe and PL emitted from the sample is collected through the same fiber. An interference filter separates QW PL emission [centered at 1.30 eV, 15 meV full width at half maximum (FWHM)] from the excitation laser. Uncoated, chemically etched near-field fiber probes are used, providing 150 nm spatial resolution and transmission efficiencies close to unity.<sup>11,12</sup> QW luminescence lifetimes are recorded with a synchroscan streak camera using a sub-100 fs Ti:sapphire laser centered at 1.57 eV as the impulsive excitation source.

Two dimensional near-field PL images  $PL(x,y)$  are recorded for different excitation powers between 3 and 300  $\mu\text{W}$  coupled into the near-field fiber probe. Images at 10 and 300  $\mu\text{W}$  are shown in Figs. 1(b) and 1(c), respectively. Strong QW PL is observed at distances  $x > 1 \mu\text{m}$  from the surface ( $x=0$ ). The PL decays gradually as the tip approaches the surface and this gradual decrease is homogeneous along the  $y$ -axis, parallel to the sample edge. It is clear that the high intensity PL [Fig. 1(c)] is spatially more uni-

<sup>a)</sup>Author to whom correspondence should be addressed: electronic mail: malyar@mbi-berlin.de

<sup>b)</sup>Permanent address: Institute of Physics, St. Petersburg State University, 198504 St. Petersburg, Russia.

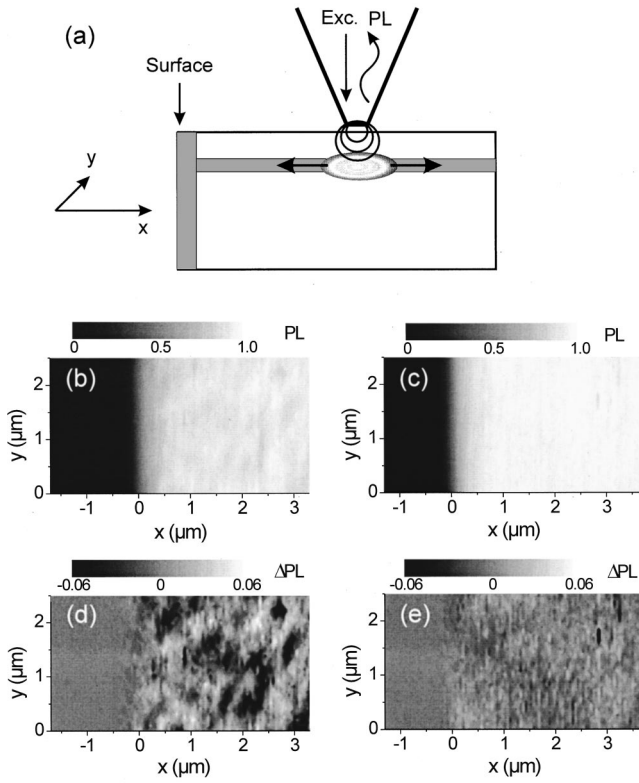


FIG. 1. (a) Schematic of the near-field PL experiment in illumination/collection geometry. The excitation laser (photon energy 1.96 eV) is transmitted through a chemically etched, uncoated near-field fiber probe. QW PL is collected through the same fiber and detected by a single photon counting system. (b) Two-dimensional, near-field QW PL intensity  $PL(x,y)$  near the edge ( $x=0$ ) of the QW sample. Excitation power  $P=10 \mu\text{W}$ .  $PL(x,y)$  is color-coded and normalized unity. (c) As (b),  $P=300 \mu\text{W}$ . (d) Line-leveled image  $\Delta PL(x,y)$  of (b),  $P=10 \mu\text{W}$ . (e)  $\Delta PL(x,y)$  of (c),  $P=300 \mu\text{W}$ .

form than the low intensity PL. Line-leveled images  $\Delta PL(x,y)$  of each figure in Figs. 1(b) and 1(e), respectively, are shown. We subtract the average value of each column and then replot the image,  $\Delta PL(x,y) = PL(x,y) - \langle PL \rangle \times(x)$ , where  $\langle PL \rangle(x)$  denotes the signal average along the y-axis. This shows strong local fluctuations in the low power PL image [Fig. 1(d)], in contrast to the almost flat high power image [Fig. 1(e)]. Such differences can be explained by the saturation of trap states at high excitation levels, as discussed below.

As the PL images are homogeneous along y, we compare in Fig. 2(a) only PL line scans along the x axis near the edge at different excitation powers. A reflectivity measurement is included (filled circles). From this curve we can deduce a spatial resolution of 140 nm in the reflectivity measurement. In all PL profiles, the PL rises much more slowly as a function of x than the reflectivity, with a characteristic length scale of about  $1 \mu\text{m}$ , approximately the diffusion length of our system. Neglecting the finite spatial resolution, the PL intensity around  $x=0$  would be zero in the limit of an infinite  $v_s$  (perfectly absorbing boundary conditions). This PL intensity should increase as  $v_s$ , making the intensity close to  $x=0$  a sensitive measure of  $v_s$ .

In order to quantitatively describe the intensity profile and to deduce  $v_s$  and  $L_D$ , we use a standard steady-state diffusion model with a boundary at  $x=0$ , where the surface recombination acts as a sink for the carriers. For excitation at

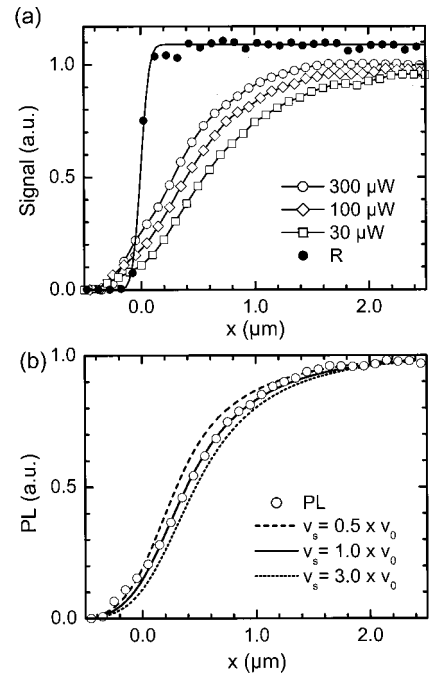


FIG. 2. (a) QW PL line scans signal recorded at different excitation densities near the sample boundary:  $P=30 \mu\text{W}$  (squares),  $100 \mu\text{W}$  (diamonds), and  $300 \mu\text{W}$  (open circles). Near-field reflectivity scan (filled circles) showing the spatial resolution of the experiment. (b) QW PL line scan for  $P=100 \mu\text{W}$  (circles), and simulations to the two-dimensional diffusion model [Eq. (1)]. Solid line:  $v_s = v_0 = 1 \times 10^6 \text{ cm/s}$ ,  $D=15 \text{ cm}^2/\text{s}$ ,  $\tau_{\text{rec}}=1.7 \text{ ns}$ . Dashed and dotted lines are for  $v_s=5 \times 10^5 \text{ cm/s}$  and  $v_s=3 \times 10^6 \text{ cm/s}$ , respectively, and the same  $D$ .

1.96 eV, electron-hole pairs are generated in the  $\text{Al}_{0.2}\text{Ga}_{0.8}\text{As}$  regions and are rapidly trapped into the QW. This trapping occurs on a time scale of few tens of ps, much faster than the QW luminescence life time  $\tau_{\text{rec}}$  of  $\sim 1 \text{ ns}$ , as confirmed by time-resolved PL. The photoexcited carriers trapped into the QW undergo diffusion within the QW plane. At room temperature, this diffusion is well described by an ambipolar diffusion model,<sup>13</sup> with a characteristic diffusion length  $L_D = \sqrt{D\tau_{\text{rec}}}$ , given by the ambipolar diffusion coefficient  $D$  and  $\tau_{\text{rec}}$ . We therefore assume identical electron and hole QW densities  $n_e^{\text{QW}} = n_h^{\text{QW}} = n$ , their spatial variation being described by the following two-dimensional diffusion equation:

$$D \left( \frac{\partial^2}{\partial x^2} + \frac{\partial^2}{\partial y^2} \right) n - \frac{n}{\tau_{\text{rec}}} + n_a g(x_0, y_0) = 0. \quad (1)$$

Here,  $g(x_0, y_0) = (1/\sqrt{2\pi}\sigma) e^{-[(x-x_0)^2 + (y-y_0)^2]/2\sigma^2}$  is a local source term, describing carrier generation by the near-field tip positioned at  $(x_0, y_0)$ . It is described by a Gaussian spatial profile<sup>14</sup> with a FWHM  $\sqrt{2 \ln(2)}\sigma$  of 300 nm. Due to finite depth of the buried QW layer, its width is larger than that deduced from the reflectivity measurement. The generated carrier density is given by the constant  $n_a$ . We solve Eq. (1) with the following boundary condition at the sink,  $x=0$ :

$$D \frac{\partial n}{\partial x} \Big|_{x=0} = v_s \cdot n.$$

The locally detected PL intensity  $PL(x_0, y_0) \propto \iint dx dy \cdot g(x_0, y_0) \cdot n$ . From the spatial variation of the PL signal alone, only two parameters, the diffusion length  $L_D$  and

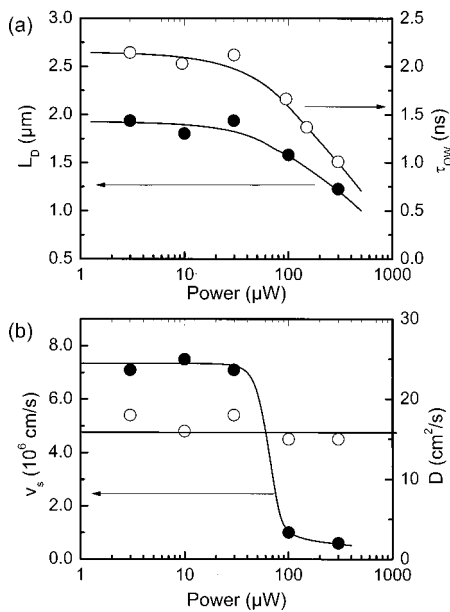


FIG. 3. (a) Diffusion length  $L_D$  (open circles) deduced from the simulation of the near-field PL line scans to the diffusion model and QW PL lifetime  $\tau_{\text{rec}}$  measured by time resolved PL spectroscopy. (b) Surface recombination velocity ( $v_s$ , filled circles) and diffusion coefficient ( $D$ , open circles), extracted from the simulation of the PL line scans using the measured values of  $\tau_{\text{rec}}$ .

product ( $v_s \cdot \tau_{\text{rec}}$ ) can be deduced. To independently extract all three parameters of the model, i.e.,  $D$ ,  $\tau_{\text{rec}}$ , and  $v_s$ , additional information is needed. Therefore, QW luminescence lifetimes  $\tau_{\text{rec}}$  are measured by time resolving the QW PL after fs-excitation at 1.57 eV [Fig. 3(a)]. Lifetimes of about 2 ns, typical for this kind of QW for diode laser applications,<sup>15</sup> are measured at low excitation densities.  $\tau_{\text{rec}}$  decreases to about 1 ns toward the high-density regime. This trend corresponds to earlier experimental results on such QW.<sup>15–17</sup>

The cross-sectional PL intensities near the edge are then compared to the simulated PL profiles using the diffusion model [Fig. 2(b)] with  $L_D$  and  $v_s \tau_{\text{rec}}$  as independent parameters. The fitting is sensitive to both  $L_D$  and  $v_s \tau_{\text{rec}}$ .  $L_D$  is mostly determined from the larger  $x$  region, whereas  $v_s \tau_{\text{rec}}$  affects the relative intensity at  $x=0$ . The sensitivity of the simulation to  $v_s$  is illustrated. Similar to the lifetime, the diffusion length is constant (2 μm) at low powers and decreases at powers of more than 30 μW. This decrease is clearly linked to the decrease in carrier lifetime. Within the experimental accuracy, the diffusion coefficient  $D \approx 16 \text{ cm}^2/\text{s}$  is density independent [Fig. 3(b)]. Using an Einstein relation,  $\mu_{\text{eff}} = eD/kT$  ( $e$  is electron charge,  $kT$  is thermal energy) one derives  $\mu_{\text{eff}} = 620 \text{ cm}^2/\text{Vs}$  at  $T = 300 \text{ K}$ . This value is close to the mobility of holes in  $\text{In}_{0.16}\text{Ga}_{0.84}\text{As}$ ,<sup>17</sup> whereas electron mobilities are much higher. We conclude that hole diffusion determines the experimentally measured diffusion length, *a posteriori* validating the assumption of an ambipolar diffusion model.

Now we discuss the values of  $v_s$  deduced from the simulation of the near-field experiments [Fig. 3(b)]. At low excitation powers  $\leq 30 \text{ μW}$ , the PL intensity around  $x=0$  is close to zero. In this regime, the sample surface can in good approximation be considered as a perfectly absorbing boundary. The value of  $v_s = 7 \times 10^6 \text{ cm/s}$  given in Fig. 3(b) is the minimum value of  $v_s$  that allows a satisfactory fit to the low

PL intensity around  $x=0$ . Clearly, our experiment is not sensitive to higher values of  $v_s$ . The experimental PL intensity at  $x=0$  increases substantially for the higher powers and hence the perfectly absorbing boundary description becomes inadequate. Values of  $v_s$  of  $1 \times 10^6$  and  $6 \times 10^5 \text{ cm/s}$  are deduced at powers of 100 and 300 μW, respectively.<sup>17</sup> This density dependence shows that the saturation of nonradiative recombination near the QW surface is the microscopic mechanism behind the decrease of  $v_s$  at high densities. It is likely that trap-like zero-dimensional centers are responsible.<sup>18</sup> Their areal density can roughly be estimated from Fig. 3(b) as  $5 \times 10^{11} \text{ cm}^{-2}$ . It is interesting that this excitation density coincides with the disappearance of the lateral intensity fluctuations in the two-dimensional near-field PL images (Fig. 1), i.e., at positions far away from the edge. Here, obviously, the microscopic mechanism causing these fluctuations is different. As  $\tau_{\text{rec}}$  varies only slightly, radiative defects arising, for example from interface roughness,<sup>19</sup> are responsible for the spatial fluctuations of the PL intensity.

In conclusion, this letter describes a technique for the simultaneous nanoscopic measurement of surface recombination velocity and diffusion constant in semiconductor nanostructures. Spatially resolved near-field PL scans at the edge of a quantum well sample are compared to a two dimensional diffusion model and  $v_s$  and  $L_D$  are deduced for various excitation powers. A pronounced decrease of  $v_s$  with increasing excitation power is a strong indication for saturation of nonradiative center near the sample surface.

Financial support by Deutsche Forschungsgemeinschaft under SFB 296, BMB+F 13N7384/8 and the European Union through the EFRE program is gratefully acknowledged. We thank D. S. Kim for stimulating discussions.

<sup>1</sup>D. E. Aspnes, Surf. Sci. **132**, 406 (1983).

<sup>2</sup>R. Schatz and C. G. Bethea, J. Appl. Phys. **76**, 2509 (1994).

<sup>3</sup>L. K. Luke, J. Appl. Phys. **90**, 3413 (2001).

<sup>4</sup>H. Hillmer, A. Forchel, T. Kuhn, G. Mahler, and H. P. Meier, Phys. Rev. B **43**, 13992 (1991).

<sup>5</sup>K. Tai, T. R. Hayes, S. L. McCall, and W. T. Tsang, Appl. Phys. Lett. **53**, 302 (1988).

<sup>6</sup>H.-C. Ostendorf and A. L. Endrös, Appl. Phys. Lett. **71**, 3275 (1997).

<sup>7</sup>S. Krawczyk, M. Bejar, A. Khoukh, R. Blanchet, B. Sermage, D. Cui, and D. Pavlidis, J. Appl. Phys. **38**, 992 (1999).

<sup>8</sup>A. J. Sabbah and D. M. Riffe, J. Appl. Phys. **88**, 6954 (2000).

<sup>9</sup>J. Shah, *Ultrafast Spectroscopy of Semiconductors and Semiconductor Nanostructures 2nd ed.*, Springer Series in Solid State Physics (Springer, Berlin, 1999).

<sup>10</sup>H. Ichikawa, K. Inoshita, and T. Baba, Appl. Phys. Lett. **78**, 2119 (2001).

<sup>11</sup>F. Intonti, V. Emiliani, C. Lienau, T. Elsaesser, V. Savona, E. Runge, R. Zimmermann, R. Nötzel, and K. H. Ploog, Phys. Rev. Lett. **87**, 076 801 (2001).

<sup>12</sup>R. Müller and C. Lienau, Appl. Phys. Lett. **76**, 3367 (2000).

<sup>13</sup>A. Richter, G. Behme, M. Süptitz, Ch. Lienau, T. Elsaesser, M. Ramsteiner, R. Nötzel, and K. H. Ploog, Phys. Rev. Lett. **79**, 2145 (1997).

<sup>14</sup>R. Müller and C. Lienau, J. Microsc. **202**, 339 (2001).

<sup>15</sup>A. P. Ongstad, D. J. Gallant, and G. C. Dente, Appl. Phys. Lett. **66**, 2730 (1995).

<sup>16</sup>R. K. Ahrenkiel, R. Ellingson, S. Johnston, and M. Wanlass, Appl. Phys. Lett. **72**, 3470 (1998).

<sup>17</sup>Internet address: <http://www.ioffe.rssi.ru/SVA/NSM/Semicond/GaInAs/>

<sup>18</sup>J. W. Tomm, A. Bärwolff, T. Elsaesser, and J. Luft, Appl. Phys. Lett. **77**, 747 (2000).

<sup>19</sup>F. Intonti, V. Emiliani, Ch. Lienau, T. Elsaesser, R. Nötzel, and K. H. Ploog, Phys. Rev. B **63**, 075 313 (2001).